Applied Physics B (2020) 126:187
https://doi.org/10.1007/s00340-020-07536-y

Applied Physics B
Lasers and Optics

Design and implementation of a tunable composite photonic crystal cavity on an optical nanofiber

Ramachandrarao Yalla[1] · Kohzo Hakuta[2]

Received: 30 November 2019 / Accepted: 8 October 2020 / Published online: 26 October 2020

Abstract
We report a novel approach to the design and implementation of a tunable cavity on an optical nanofiber (ONF). The key point is to create a composite photonic crystal cavity (CPCC), by combining an ONF and a diverged period defect mode grating. Using numerical simulations we design the CPCC with low scattering loss while tuning the cavity resonance wavelength of ±10 nm around the designed wavelength. We experimentally demonstrate the tunability of the CPCC, showing good agreement with the simulation results. Our results lay the foundation for a versatile platform for ONF cavity-quantum-electrodynamics with narrow bandwidth quantum emitters.

Keywords Nanophotonics and photonic crystals · Photonic crystal waveguides

1 Introduction

Nano-waveguides offer a versatile and growing platform for nano-photonics with various applications, typically in quantum optics [1–6], quantum photonics [7], and sensing [8, 9]. Cavity creation on nano-waveguides is a crucial requirement for enhancing the light-matter interaction strength. To date, various approaches have been developed by directly fabricating nanostructures on the nano-waveguide itself [10–13]. From the viewpoint of fiber networks, tapered optical fibers with sub-wavelength in diameter termed as optical nanofibers (ONFs) are particularly promising due to their ability of automatic coupling to single mode fibers [1–5].

Cavity formation on the ONF has been demonstrated via two methods: one is the direct fabrication of photonic crystal cavities on the ONF itself using focused ion beam milling technique and femtosecond laser ablation [10, 14–18] and the other is a composite photonic crystal cavity (CPCC) method, which does not directly fabricate on the ONF. The CPPC was formed by mounting the ONF onto a nanofabricated grating with a central defect [19, 20, 22]. To extend such ONF cavities for cavity quantum electrodynamics (QED), one crucial requirement is the ability to tune the cavity resonance wavelength (λ_{res}) precisely to match with the narrow spectral emission line of a quantum emitter. Regarding the direct fabrication methods, tuning the λ_{res}-value up to ±10 nm around the designed wavelength has been experimentally demonstrated by mechanical stretching of the ONF [15, 16]. Regarding the composite method, although the tuning of the λ_{res}-value has not been experimentally demonstrated, two possible ways have been proposed. One is to precisely control the ONF diameter so that the effective refractive index of the ONF guided mode changes. The other is by changing the relative angle (θ) between the ONF and the defect mode grating (DMG) [20]. The precise control of the ONF diameter can be achieved via tensile and smooth tapered properties of the ONF. However, to tune the λ_{res}-value up to ±10 nm, the expected ONF diameter variation should be ±6% [20, 22], leading to exceed the limit of tensile property of the ONF which may result in ONF break during the experiments. The smooth tapered ONF is not preferable, in the context of working with a solid state quantum emitter as it is deposited at a specific location on the surface of the ONF. The precise control of the θ-value can be achieved via the rotation of either the ONF or the DMG. The required θ-value should be ±10° to tune the λ_{res}-value up to ±10 nm, leading to an increase of the scattering

✉ Ramachandrarao Yalla
ramu@uohyd.ac.in

Kohzo Hakuta
k.hakuta@cpi.uec.ac.jp

1 School of Physics, University of Hyderabad, Hyderabad, Telangana 500046, India

2 Center for Photonic Innovations, University of Electro-Communications, Chofu, Tokyo 182-8585, Japan

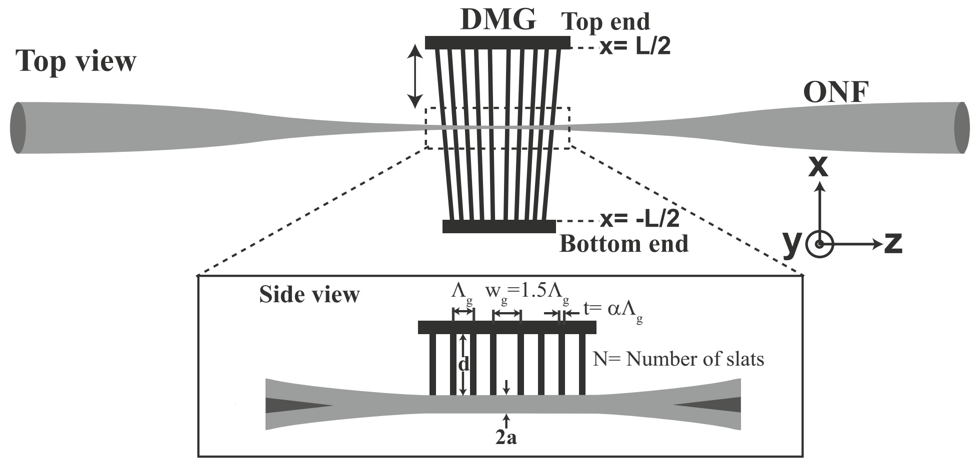

Fig. 1 A conceptual top view of a tunable composite photonic crystal cavity (CPCC). The tunable CPCC is formed by an optical nanofiber (ONF) and a diverged period defect mode grating (DMG). The bottom end and top end correspond to $x = -250$ μm ($-L/2$) and x= 250 μm ($L/2$), respectively. The inset shows a conceptual side view of the tunable CPCC with defined parameters

loss and resulting degradation in the performance over the tuning range.

In this paper, we investigate a systematic design and implementation of tunable CPCC on the ONF, by combining the ONF and a diverged period DMG. As conceptually displayed in Fig. 1, top view, the essential point of the idea is to fabricate the DMG, the grating period of which is varied linearly from the bottom end to the top end. By changing the mounting position of the DMG onto the ONF from a minimum period position (bottom end) to a maximum period position (top end), the created CPCC λ_{res}-value can be tuned from one wavelength corresponding to the minimum grating period to another wavelength corresponding to the maximum grating period.

2 Tunable CPCC parameters design procedure

We describe the design of a diverged period DMG and created CPCC. Here we restrict the discussion to a symmetric cavity structure. The directions x, y, and z are defined as shown in Fig. 1. The essential parameters are schematically illustrated in the inset of Fig. 1, side view. Design parameters for the present CPCC are ONF diameter ($2a$), grating period (Λ_g), defect-width (w_g)= $1.5\Lambda_g$, duty cycle (α), slat width (t)= $\alpha\Lambda_g$, and number of slats (N). We assume a rectangular slat shape with a slat depth (d) of 2 μm. In the present design, we set the DMG length (L) to be 500 μm. The DMG center is $x = 0$. The bottom end and the top end correspond to $x = -250$ μm ($-L/2$) and $x = 250$ μm ($L/2$), respectively. As conceptually depicted in Fig. 1, the position (x) where the DMG touches (attaches) the ONF is defined as the mounting position (x_m). Thus, the $x_m = -250$ μm, x_m= 0, and x_m= 250 μm correspond to the bottom end, center, and the top end, respectively. We design the present CPCC tunability of $\pm$10 nm around a specific wavelength at the center wavelength of 640 nm. The Λ_g-value must varied linearly by $\pm$5 nm over the DMG length from the bottom end to the top end. To achieve this condition, the angle difference between the center slat and the furthest was set to a value of 0.17°, leading to a negligible change in the scattering loss over the tuning range as in the case of parallel-slat DMGs.

Using the finite difference time domain (FDTD) method, we find the optimum parameters for the CPCC by simulating the channeling efficiency (η) into the ONF guided modes [20]. The key point of the optimization is to choose the optimum ONF diameter ($2a$), minimum reproducible slat width (t) for fabrication, and small slat angle (θ_s) for wider tunability while keeping the scattering loss as small as possible over the tuning range. We set a y-polarized dipole source on the surface of the ONF as it is expected to have maximum η -value. The parameter optimization procedure is as follows: according to Bragg resonance condition, λ_{res}= $2n_{eff}\Lambda_g$, where n_{eff} is the effective refractive index of the fundamental mode of the nanofiber and Λ_g is the grating period. The effective refractive index depends on the nanofiber diameter ($2a$), the refractive indices of the core (~ 1.45) and clad (~ 1), and the wavelength of the light. We assume the slat width (t= $\alpha\Lambda_g$) to be around 50 nm due to fabrication reliability as discussed in the Refs. [19, 20]. From the above, we obtain the relation $n_{eff}/\alpha = \lambda_{res}/100$. The obtained n_{eff}/α -value to be around 8 assuming λ_{res}-value to be 800 nm as discussed in Ref. [20]. The expected α-value range would be 12.5–18.0% assuming the n_{eff}-value range to be 1–1.45. We simulated η-values for various n_{eff}-values i.e. various $2a$-values (fiber size parameters, k_0a) to obtain the maximum η-value, while keeping the α-value at 15% (average value of

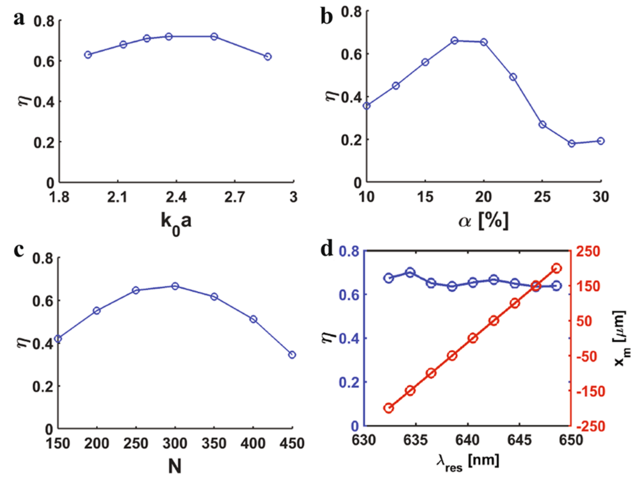

Fig. 2 **a** Simulation predicted values for the channeling efficiency (η) as a function of fiber size parameter (k_0a). **b** η-value dependence on the duty cycle (α) of the DMG. **c** η-value dependence on the number of slats (N) of the DMG. **d** η-value (blue) and x_m-value (red) versus cavity resonance wavelength (λ_{res})

the range). It should be mentioned that Λ_g-value is chosen to produce λ_{res}-value at the designed wavelength and also N-value is swept to optimize the η-value. The summary of such results for the η-values versus k_0a-values are plotted in Fig. 2a. One can readily see that η-value is almost uniform over the k_0a-value from 2.2 to 2.6. We set the k_0a-value to be 2.5 to minimize the scattering loss due to the fabricated slat shape deviation from a rectangular shape as discussed in Ref. [20]. Assuming the design wavelength to be around 640 nm, the corresponding $2a$-value is 510 nm. Note that the optimum parameters are governed by the $\frac{a}{\lambda}$-value, not by the wavelength (λ) itself.

For the current design, the obtained n_{eff}/α-value is around 6.4 assuming the λ_{res}-value to be 640 nm. The expected α-value range would be 15.5–22.5%. By monitoring the η-value at x_m= 0, the α-value is swept by 10–30%, while keeping $2a$-value fixed at 510 nm i.e. n_{eff}-value is fixed. The simulated results are plotted in Fig. 2b, the optimum α-value is found to be around 20%. The N-value is swept from 150–450, while keeping the α-value at the optimum. The simulated results are plotted in Fig. 2c, the optimum N-value is found to be around 300. The Λ_g-value is swept to produce the designed λ_{res}-value (640 nm) and it is found to be 252 nm. Thus, the minimum and maximum Λ_g-values are 247 nm (bottom end) and 257 nm (top end), respectively. Note that the angle difference between the center slat and the furthest slat is quite small 0.17°, leading to a negligible change in the scattering loss from parallel-slat DMGs. We also examined the η-value at various mounting positions (x_m) i.e. various λ_{res}-values. The summary of the simulated results are plotted in Fig. 2d. The blue and red circles correspond to η-values and x_m-values, respectively. Regarding η-value versus λ_{res}-value, one can readily see the uniform behavior over the tuning range, suggesting the stable performance of the present CPCC thanks to the small slat angle. Regarding x_m-value versus λ_{res}-value, one can readily see the linear behavior as expected. Thus, we set the tunable CPCC parameters as follows: $2a$= 510 nm, Λ_g= 252 (±5) nm, w_g= 378 (±7.5) nm, α= 20%, t = 50.4 (±1.0) nm, and N = 300. We design the present CPCC tunability of ±10 nm around a center wavelength of 640 nm, assuming a colloidal quantum dot as a quantum emitter, the centre wavelength of which may vary about ±10 nm [21].

3 Experimental procedure

Based on the optimized parameters discussed above, diverged period DMG patterns were fabricated on a silica substrate using electron beam lithography along with chemical etching [19, 20]. The ONF was fabricated using a heat and pull technique [17, 22]. The diameter of the ONF was 515±5 nm and was uniform for 2.5 mm in the waist region. The optical transmission through the ONF was 97%. The ONF was placed at the focus point of an inverted microscope using a high precision *xz*-stage. By observing the DMG pattern using a CCD camera, the ONF was positioned perpendicular to the slats using a rotational stage. The waist part of the ONF was found by measuring the tapering behavior of the ONF. Details can be found in Refs. [19, 20]. The position of the x_m= 0 was determined by finding the top and bottom edge of the DMG pattern.

The experimental setup for the optical characterization of the present CPCC is shown in Fig. 3. We inject a spectrally filtered supercontinuum light with an output wavelength ranging from 600 to 700 nm. The light is directed through a polarizer (P) to ensure linear polarization. The injected light polarization angle is controlled via a fiber in-line polarizer (ILP). The resultant cavity transmission spectrum is measured using a spectrum analyzer (SA) with a resolution of 0.05 nm.

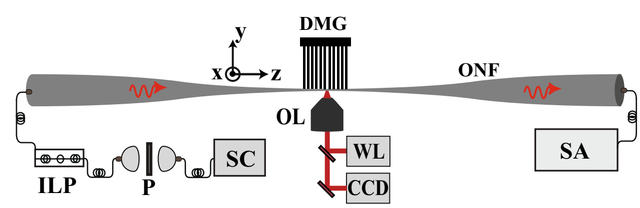

Fig. 3 The experimental setup for measuring the cavity transmission spectrum. SC, P, ILP, OL, WL, CCD, and SA denote super-continuum source, polarizer, in-line polarizer, objective lens, white light source, charge-coupled device, and spectrum analyzer, respectively

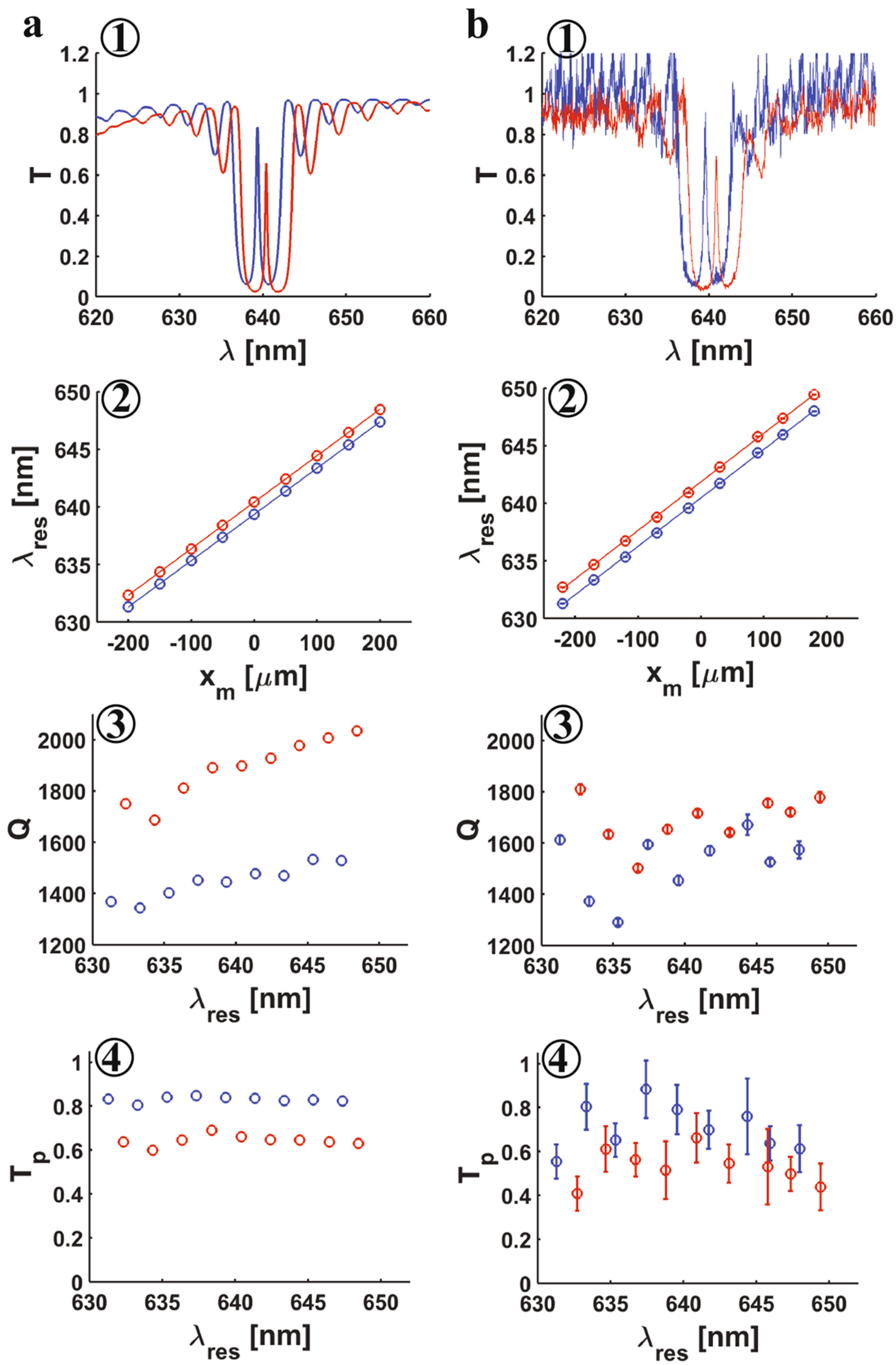

Fig. 4 Simulated and corresponding measured results for a tunable composite photonic crystal cavity (CPCC): **a** Simulated results are labeled from 1 to 4. **a1** Cavity transmission spectra for the x (blue trace) and y (red trace)-modes at the mounting position (x_m)= 0, respectively. **a2** Cavity resonance wavelength (λ_{res}) as a function of x_m-values. Blue (red) circles correspond to the x (y)-mode. Blue (red) solid line is a linear fit to the x (y)-mode λ_{res}-values. **a3**, **a4** are the obtained quality factor (Q) and peak transmission (T_p) versus λ_{res}-values, respectively. In both the plots, blue (red) circles correspond to the x (y)-mode. **b** The measured results corresponding to the simulation predicted results are labeled from 1 to 4. **b1** Cavity transmission spectra for the x (blue trace) and y (red trace)-modes at x_m= −20 μm, respectively. **b2** The λ_{res}-values as a function of x_m -values. Blue (red) circles correspond to the x (y)-mode. Blue (red) solid line is a linear fit to the x (y)-mode λ_{res}-values. **b3**, **b4** show the obtained Q-values and T_p-values versus λ_{res}-values, respectively. In both the plots, blue (red) circles correspond to the x(y)-mode

4 Simulation and experimental results

The simulated and measured tunable CPCC characteristics are shown in Fig. 4a, b, respectively. We simulated the cavity transmission spectra at various mounting positions (x_m) with a step size of ±50 μm from the x_m= 0. In Fig. 4a1, we show a typical simulated cavity transmission spectra for both x- and y-polarizations at x_m= 0. Blue (red) trace corresponds to the x (y)-polarization. For both the traces, one can readily see a strong photonic stop-band at 640 nm along with a peak at the center. Due to the asymmetrical index modulation, the degeneracy of the x- and y-polarized fundamental modes of the ONF is lifted. The λ_{res}-value is found to be 639.36 nm (640.42 nm) for the x (y)-mode. The x- and y-modes resonance peaks are separated by 1.06 nm. The obtained values of quality factor (Q) and peak transmission (T_p) are 1443 (1898) and 0.84 (0.66) for the x (y)-mode, respectively. The y-mode has a higher Q (lower T_p)-value than the x-mode due to the fact that y-mode experiences more stronger modulation, leading to a higher reflectivity (scattering loss). We compared the present simulated values to those values obtained for the non-tilted slats at the same designed wavelength. Note that any apparent performance degradation was not observed.

We mount the DMG around the center of the pattern i.e. $x_m = 0$ to produce the λ_{res}-value around the designed wavelength (640 nm). The measured cavity transmission spectra corresponding to the simulated spectra is shown Fig. 4b1. The measured cavity transmission spectra correspond to the x_m-value of −20 μm. Blue (red) trace corresponds to the x (y)-mode. In both the traces, we observed a strong optical stop-band at a wavelength of 640 nm accompanied by a single peak at the center as predicted by the simulations. The peak corresponds to the λ_{res}-value of 639.57 nm (640.90 nm) for the x (y)-mode. The separation in λ_{res}-values for the x- and y-modes is 1.33 nm. The obtained values of Q and T_p are 1453±20 (1715±15) and 0.79±0.11 (0.66±0.06) for the x (y)-mode, respectively. The measured stop-band, clear polarization dependence, and cavity mode around the designed wavelength (640 nm) behavior reproduce the simulation results as shown in Fig. 4a1. Note that the measured λ_{res}-value, Q-value, and T_p-value for the x- and y-modes are in good quantitative agreement with the simulation predicted values.

The simulated tunability of the present CPCC i.e. the obtained λ_{res}-values as a function of x_m-values are plotted in Fig. 4a2. Blue (red) circles correspond to the x (y)-mode. The λ_{res}-value increases linearly with the x_m-value. This is due to a linear variation of the Λ_g-value from the bottom end to the top end of the DMG. We fit a linear function to the simulation predicted values. The fitted result for the x (y)-mode λ_{res}-values is shown by blue (red) solid line. For the x (y)-mode, the obtained slope (S) and resonance wavelength (λ_0) at $x_m = 0$ are 0.0401 nm/μm (0.0404 nm/μm) and 639.34 nm (640.40 nm), respectively.

We measured the cavity transmission spectra at various x_m-values. It should be mentioned that the composite system is mechanically stable because the ONF sticks to the DMG via Van der Waals force. Therefore, for the tuning we unmounted (detached) the DMG from the ONF at $x_m = -20$ μm and translated the DMG position along the x-axis with a step size of ±50 μm for next mounting. The experimentally measured tunability behavior corresponding to the simulation result is shown in Fig. 4b2. Blue (red) circles correspond to the x (y)-mode. One can readily see a linear dependence of the λ_{res}-values for the x (y)-mode as predicted by the simulations. We obtained S-value and λ_0-value, by fitting a linear function to the measured data. Blue (red) solid line is the fitted result for the x (y)-mode λ_{res}-values. For the x (y)-mode, the obtained S-value and λ_0-value are 0.0416 nm/μm (0.0422 nm/μm) and 640.42 nm (641.84 nm), respectively. Note that the measured λ_{res}-values for the x (y)-mode behavior reproduced the simulation predicted behavior as shown in Fig. 4a2. We measured the tunability behavior for the nine DMG patterns using the same ONF. We found mean values of S and λ_0 are 0.04190±0.00032 nm/μm (0.04210±0.00015 nm/μm) and 640.57 ±0.16 nm (642.09±0.21 nm) for the x (y)-mode, respectively.

Next, we show the performance stability of the present CPCC over the tuning range. The obtained Q-values against λ_{res}-values are plotted in Fig. 4a3. Blue (red) circles correspond to the x (y)-mode. The Q-value increases with the λ_{res}-value from 1368 (1750) to 1528 (2035) for the x (y)-mode. The obtained Q-values show fluctuation around the mean value of 1446±65 (1887±117) for the x (y)-mode.

The measured Q-value versus λ_{res}-value corresponding to the simulation predicted values are shown in Fig. 4b3. Blue (red) circles correspond to the x (y)-mode. The vertical error bars are due to the fluctuations in the λ_{res}-value and the cavity mode width. The measured Q-values show fluctuation around the mean value of 1517±122 (1689±93) for the x (y)-mode. The measured Q-values for the y-mode are higher than the x-mode as predicted by the simulations. The measured behavior reproduced the simulation predicted results as shown in Fig. 4a3. Note that cavity finesse can be estimated to be 25(±2) using the measured cavity mode width and effective cavity length of 22 μm.

The simulated T_p-values versus the λ_{res}-values are plotted in Fig. 4a4. Blue (red) circles correspond to the x (y)-mode. The T_p-value is almost kept constant over the tuning range for the x (y)-mode, suggesting stable performance of the present CPCC owing to the small slat angle. Note that the uniform variation of the slat width (t) and the defect-width (w_g) from the bottom end to the top end of the DMG, leading to uniform scattering loss over the tuning range. The obtained T_p-values show fluctuation around a mean value of 0.83 ± 0.01 (0.64 ± 0.02) for the x (y)-mode.

The measured T_p-values versus λ_{res}-values corresponding to the simulation predicted values are shown in Fig. 4b4. Blue (red) circles correspond to the x (y)-mode. The vertical error bars are mainly due to the fluctuations in the injected source used for the measurement. The measured T_p-values show fluctuation around the mean value of 0.71 ± 0.10 (0.53 ± 0.08) for the x (y)-mode. The measured T_p-values for the y-mode are lower than the x-mode as predicted by the simulations.

5 Discussion

Regarding the slope of the cavity tuning, S, the deviation from the simulation predicted value is about 4.5% (4.2%) for the x (y)-mode. This may be due to the fabrication imperfections in the grating period (Λ_g) of the DMG. Regarding the λ_0-value, the discrepancy from the simulation predicted value is about 1.23 nm (1.69 nm) for the *x* (*y*)-mode. This may be due to the fabrication fluctuations in the nanofiber diameter (2*a*) and the Λ_g-value. We measured the 2*a*-value using scanning electron microscope and confirmed it to be close to the simulation set value of 510 nm. It should be mentioned that the measurement accuracy in 2*a*-value is ± 5 nm. Using the measured λ_0-values and assuming the fluctuations in the Λ_g-value to be around ± 0.5 nm, we estimate the 2*a*-value to be 514 ± 4 nm [20, 22]. This implies that the nanofiber diameter (2*a*) is thicker than the simulation set value.

Regarding the separation in λ_0-values for the *x*- and *y*-modes, the discrepancy from the simulation predicted value is about 0.4 nm. This may be due to thicker nanofiber diameter, which was used for current experiments. Simulations suggest that the separation is dependent on the 2*a*-value. By setting the 2*a*-value to be 520 nm, the simulation predicted value for the separation is 1.49 nm.

Although the experimental discrepancies exist, it should be mentioned that the obtained *S*-value and λ_0-value are in good agreement with the simulation predicted values within the experimental errors. The measured and simulation results clearly demonstrate that the tunability for the present CPCC is about ±10 nm around the designed wavelength of 640 nm.

Regarding the measured *Q*-values, the deviation from the simulation predicted values are about 1–17% (3–17%) for the *x* (*y*)-mode. This may be due to the fabrication fluctuation in the slat width (*t*) and the defect-width (w_g) over the DMG length, leading to a non-uniform scattering loss. Although the measured *Q*-value behavior for the *x* and *y*-modes qualitatively reproduced the simulation predicted behavior, quantitatively the observed difference in the measured *Q*-value between the *x* and *y*-mode was smaller than the expected difference. This may be due to the uncertainties involved in the experiments, originating from the fabrication uncertainties in both the slat width and the defect-width over the DMG length and the polarization uncertainty in the cavity. The measured T_p-values are deviated from the simulation predicted values by about 1–33% (1–36%) for the *x* (*y*)-mode. This may be due to the fabrication imperfections in the slat width (*t*) and the defect-width (w_g) over the DMG length, leading to a non-uniform scattering loss. Although the fluctuations in the measured results exists, the simulation and experimental results clearly demonstrate that the stable performance of the present CPCC over the tuning range.

Using the measured *S*-value, we estimate the precision of the tuning is 7.6 GHz (10.4 pm), considering the ONF movement resolution along the *x*-axis to be 250 nm. The tuning precision can be improved by increasing the ONF movement resolution. Note that the current tuning precision is about 1/35 factor of the measured cavity *y*-mode width (0.374 nm). We believe that such tuning precision value would be good enough to perform any cavity-QED experiments. On the other hand, for some applications wider tunability would be required. Simulations suggest that a slat tilt angle up to 0.51° can still keep the non-degrading performance in terms of quality factor and cavity mode transmission over the tuning range. We can tune the cavity resonance wavelength up to ± 30 nm around 640 nm using the slat angle of 0.51°. One can realize the tuning of ±50 nm using a slat tilt angle of 0.85°. In this case, however the cavity peak transmission value would be reduced.

6 Summary

In this paper, we have demonstrated the design and implementation of tunable composite photonic crystal cavity on an optical nanofiber. The numerical and experimental results have clearly shown that the composite cavity method can be extended to a tunable cavity scheme without suffering from any additional scattering loss. Experimental results have reproduced the simulated results successfully. Although discussions were restricted to a symmetric cavity structure, this method can be extended to any asymmetric cavity structure, such as one-side cavity. The present method can readily be applied to ONF cavity-QED works with narrow bandwidth quantum emitters such as laser cooled atoms [23], quantum dots at cryogenic temperatures [21, 24], and silicon vacancy centers in nano-diamonds [25], and may open new avenues and lay a versatile platform in the fields of quantum optics and nano-photonics.

Acknowledgements This work was supported by the Japan Science and Technology Agency (JST) as one of the strategic innovation projects.

Compliance with ethical standards

Conflict of interest The authors declare that they have no conflict of interest.

References

1. F.L. Kien, S. Dutta Gupta, V.I. Balykin, K. Hakuta, Phys. Rev. A **72**, 032509 (2005)
2. K.P. Nayak, K. Hakuta, New J. Phys. **10**, 053003 (2008)
3. E. Vetsch, D. Reitz, G. Sagué, R. Schmidt, S.T. Dawkins, A. Rauschenbeutel, Phys. Rev. Lett. **104**, 203603 (2010)
4. A. Goban, K.S. Choi, D.J. Alton, D. Ding, C. Lacroute, M. Pototschnig, T. Thiele, N.P. Stern, H.J. Kimble, Phys. Rev. Lett. **109**, 033603 (2012)
5. R.R. Yalla, F.L. Kien, M. Morinaga, K. Hakuta, Phys. Rev. Lett. **109**, 063602 (2012)

6. S.-P. Yu et al., Appl. Phys. Lett. **104**, 111103 (2014)
7. K.P. Nayak, M. Sadgrove, R.R. Yalla, F.L. Kien, K. Hakuta, J. Opt. **20**, 073001 (2018)
8. M.J. Morrissey, K. Deasy, M. Frawley, R. Kumar, E. Prel, L. Russell, V.G. Truong, S.N. Chormaic, Sensors **13**, 10449 (2013)
9. J. Lou, Y. Wang, L. Tong, Sensors **14**, 5823 (2014)
10. K.P. Nayak, F.L. Kien, Y. Kawai, K. Hakuta, K. Nakajima, H.T. Miyazaki, Y. Sugimoto, Opt. Express **19**, 14040–14050 (2011)
11. J.D. Thompson, T.G. Tiecke, N.P. de Leon, J. Feist, A.V. Akimov, M. Gullans, A.S. Zibrov, V. Vuletic, M.D. Lukin, Science **340**, 1202 (2013)
12. J.M. Hausmann, B.J. Shields, Q. Quan, Y. Chu, N.P. de Leon, R. Evans, M.J. Burek, A.S. Zibrov, M. Markham, D.J. Twitchen, H. Park, M.D. Lukin, M. Loncăr, Nano Lett. **13**, 5791 (2013)
13. A. Goban, C.-L. Hung, S.-P. Yu, J.D. Hood, J.A. Muniz, J.H. Lee, M.J. Martin, A.C. McClung, K.S. Choi, D.E. Chang, O. Painter, H.J. Kimble, Nat. Commun. **5**, 4808 (2014)
14. K.P. Nayak, K. Hakuta, Opt. Express **21**, 2480 (2013)
15. K.P. Nayak, P. Zhang, K. Hakuta, Opt. Lett. **39**, 232 (2014)
16. A.W. Schell, H. Takashima, S. Kamioka, Y. Oe, M. Fujiwara, O. Benson, S. Takeuchi, Sci. Rep. **5**, 9619 (2015)
17. J. Keloth, K.P. Nayak, K. Hakuta, Opt. Lett. **42**, 1003 (2017)
18. W. Li, J. Du, V.G. Truong, S. Nic Chormaic, Appl. Phys. Lett. **110**, 253102 (2017)
19. M. Sadgrove, R.R. Yalla, K.P. Nayak, K. Hakuta, Opt. Lett. **14**, 2542 (2013)
20. R.R. Yalla, M. Sadgrove, K.P. Nayak, K. Hakuta, Phys. Rev. Lett. **113**, 143601 (2014)
21. K.M. Shafi, W. Luo, R.R. Yalla, K. Iida, E. Tsutsumi, A. Miyanaga, K. Hakuta, Sci. Rep. **8**, 13494 (2018)
22. J. Keloth, M. Sadgrove, R.R. Yalla, K. Hakuta, Opt. Lett. **40**, 4123 (2015)
23. M. Sadgrove, K.P. Nayak, New J. Phys. **19**, 063003 (2017)
24. L. Biadala, Y. Louyer, B. Ph Tamarat, Phys. Rev. Lett. **103**, 037404 (2009)
25. E. Neu, D. Steinmetz, J. Riedrich-Moller, S. Gsell, M. Fischer, M. Schreck, C. Becher, New J. Phys **13**, 025012 (2011)